Environmental Pollution 253 (2019) 39–48

Contents lists available at ScienceDirect

Environmental Pollution

journal homepage: www.elsevier.com/locate/envpol

Membrane-supported 1D MOF hollow superstructure array prepared by polydopamine-regulated contra-diffusion synthesis for uranium entrapment☆

Boxuan Yu [a], Gang Ye [a, b], Jing Chen [a, b, *], Shengqian Ma [c]

[a] Collaborative Innovation Center of Advanced Nuclear Energy Technology, Institute of Nuclear and New Energy Technology, Tsinghua University, Beijing, 100084, China
[b] Beijing Key Lab of Radioactive Waste Treatment, Tsinghua University, Beijing, 100084, China
[c] Department of Chemistry, University of South Florida, 4202 E. Fowler Avenue, Tampa, FL, 33620, United States

ARTICLE INFO

Article history:
Received 4 May 2019
Received in revised form
14 June 2019
Accepted 27 June 2019
Available online 28 June 2019

Keywords:
Metal-organic frameworks
Polydopamine
Uranium
Track-etched membrane
Separation

ABSTRACT

This work reports the architecture of a novel class of membrane-supported 1D MOF hollow superstructures, by using the bio-inspired polydopamine (PDA) mediated contra-diffusion synthetic strategy, for facile and efficient separation of uranium in a flow-through mode. PDA chemistry was firstly employed to modify the inner surfaces of the cylindrical pore channels of polycarbonate track-etched membrane (PCTM), thereby regulating the heterogeneous nucleation and interfacial growth of ZIF-8 crystals. ZIF-8 hollow superstructures embedded in membrane matrix with well-defined 1D channels were obtained. These membrane-supported MOF hollow superstructures then, for the first time, served as integrated chromatographic micro-column arrays for effective entrapment of uranium from aqueous solutions. It is highlighted that the PCTM supported ZIF-8 superstructures exhibited outstanding uranium entrapment ability in both traditional batch mode (capacity 62.3 mg/g) and fast flow-through mode (removal rate over 90% for 3 level). Moreover, new insights into the interaction between ZIF-8 and uranyl ions were obtained, suggesting that an ion-exchange mechanism involved synergistic effect was responsible for uranium binding, especially in a long-term exposure. The membrane-supported 1D MOF hollow superstructures developed in this work represent a new category of organic-inorganic composite membrane. And, it is envisioned that the methodology established in this work would be versatile for preparing more MOF superstructures with deployable form for separation applications.

In summary, a novel class of membrane-supported ZIF-8 hollow superstructure was fabricated for effective separation of uranyl ions.

1. Introduction

Metal-organic frameworks (MOFs) are a series of crystalline porous hybrid materials with ordered three-dimensional (3D) structures consisting of metal ions or cluster as nodes and organic ligands as spokes *via* coordination bonds (Furukawa et al., 2014; He et al., 2014; Li et al., 2016). Because of the controlled porosity, high crystallinity and task-specific designability (Zhang and Zaworotko, 2014), MOFs have emerged as one of most attractive materials in recent decades holding bright prospects for application in many fields, including gas adsorption and storage (Al-Maythalony et al., 2017; Cui et al., 2016; Li et al., 2009), environmental remediation (Chen et al., 2017; Kalmutzki et al., 2018; Zhu et al., 2017), catalysis (Deria et al., 2016; Li et al., 2015), and drug delivery (Wu and Yang, 2017; Zhe et al., 2018). In particular, MOFs have attracted much attention in the capture of metal ions from aqueous environment (Wang et al., 2019) due to their inherent coordinating ability of the functional groups, such as amines, carboxylates and sulfonates in the organic ligands (Li et al., 2018). Researchers have devoted substantial efforts to synthesize new MOFs or to modify existing MOFs for the entrapment of specific ions (Chen et al., 2017; Feng

☆ This paper has been recommended for acceptance by Dr. Sarah Harmon.

* Corresponding author. Collaborative Innovation Center of Advanced Nuclear Energy Technology, Institute of Nuclear and New Energy Technology, Tsinghua University, Beijing, 100084, China.
E-mail addresses: yegang@mail.tsinghua.edu.cn (G. Ye), jingxia@tsinghua.edu.cn (J. Chen).

https://doi.org/10.1016/j.envpol.2019.06.114
0269-7491/

et al., 2013; Maleki et al., 2015; Peng et al., 2016; Wu et al., 2018). As a kind of solid phase extraction materials (Sun et al., 2018; Wang et al., 2018), MOFs demonstrate the advantages of low energy cost and high selectivity (Płotka-Wasylka et al., 2016). Despite of their advantages, there remains a pressing challenge for the application of MOFs due to the lack of a conveniently deployable form (Falcaro et al., 2014). The typical powder crystal morphology always makes MOFs difficult and tedious to separate from liquid phase. Therefore, integrating MOFs with other supporting matrix represents a promising strategy to prepare MOF-based adsorption materials, which combines the advantages of each component, endowing the composites with improved synergistic effects (Lu et al., 2012; Min et al., 2017).

Diverse forms of candidate supporting materials to accommodate MOFs for preparing functional composites include particles (Dargahi et al., 2017; Ehrling et al., 2018), fibers (Jian et al., 2016), membranes (Meimei et al., 2015), and bulk matrix (Zhuang et al., 2011). Among these matrix materials, membranes stand out by the feature of superb handling capacity, small footprint, and relatively low costs (Huang et al., 2009; Koushkbaghi et al., 2018). The combination of MOFs and membrane technology solves the problems of solid-liquid separation as well as low capacity of matrix materials, which is a common strategy to prepare gas separation membrane (Huang et al., 2015; Liu et al., 2013) and, in theory, can also be promising as an alternative method for the treatment of metal ions-containing water (Na et al., 2016). To introduce MOFs to membrane matrix, surface functionalization and pore channel modification are the two major strategies. The former usually requires rigid matrix with relatively strong interactions, which is appropriate for the functionalization of inorganic membranes and sieving filtration rather than adsorption filtration (Huang et al., 2014). On the contrary, the latter shows more stable and higher load amount of MOFs but demands precise interface regulation to prevent blocking of the pore channels of membranes or the loss of MOFs (Knebel et al., 2018).

To establish robust interaction between MOFs and matrix materials, it is critical to regulate the nucleation and growth behavior of MOFs on the interfaces (Meimei et al., 2015; Norbert and Shyam, 2011). Polycarbonate track-etched membrane (PCTM) is a kind of ultrafiltration membrane that has standard cylindrical channels spanning across the structure with random distribution (Apel, 2001; Fleischer and Price, 1964). Due to the unique structure and compatibility to organic precursor of MOFs, PCTM provides an ideal porous platform enabling the controllable growth of MOF crystals inside the pore channels (Chizallet et al., 2010; Yu et al., 2018). Basically, the nature of the interface notably influences the growth behavior of the MOF crystals. In this respect, the mussel-inspired polydopamine (PDA) chemistry (Lee et al., 2007) developed in recent years offers a favorable tool for pore channel modification of PCTM, which can regulate the heterogeneous nucleation and interfacial growth of various MOFs for architecture of one-dimensional (1D) superstructures. It is envisioned that these membrane supported MOF superstructures with hierarchical porosity would find better applications in corresponding areas than MOFs with the native powder form.

Uranium as the most critical ingredient for the production of nuclear power is being extensively consumed nowadays (Bone et al., 2017). Except the limited uranium reserves in traditional mines, considerable amounts of uranium from aqueous environment, such as uranium-containing wastewater (Gill et al., 2016) and ocean water (Abney et al., 2017; Sugasaka et al., 1981), are gradually attracting people's attention in recent years (Chu and Majumdar, 2012). With these prospects in mind, it is crucial to develop a method to separate the uranium from aqueous environment in cost- and energy-efficient ways.

Herein, we present, for the first time, the robust PCTM supported 1D MOF hollow superstructures prepared by PDA mediated contra-diffusion synthesis for facile and effective uranium entrapment (Scheme 1). The bio-inspired PDA chemistry was firstly utilized to modify the inner surfaces of the pore channels, which provided anchoring sites of MOF crystals and worked as interfacial 'cement' to stabilize the MOF superstructures. Due to the well-defined structure and affinity to uranyl ions, ZIF-8 was then chosen as a prototypical MOF in-situ grown in the uniform pore channels of PCTM. It is highlighted that the 1D ZIF-8 hollow superstructures could serve as micro-scaled chromatographic column arrays for separating uranium from aqueous solution quickly and efficiently. Outstanding adsorption properties of the PCTM supported ZIF-8 superstructures were demonstrated in both traditional batch mode (capacity 62.3 mg/g) and fast flow-through mode (removal rate over 90% for 3 level). Moreover, the composite membrane can be regenerated by 0.1 mol/L sodium carbonate solution in flow through mode and reused for over 7 times without obvious capacity degradation. Besides, an ion-exchange

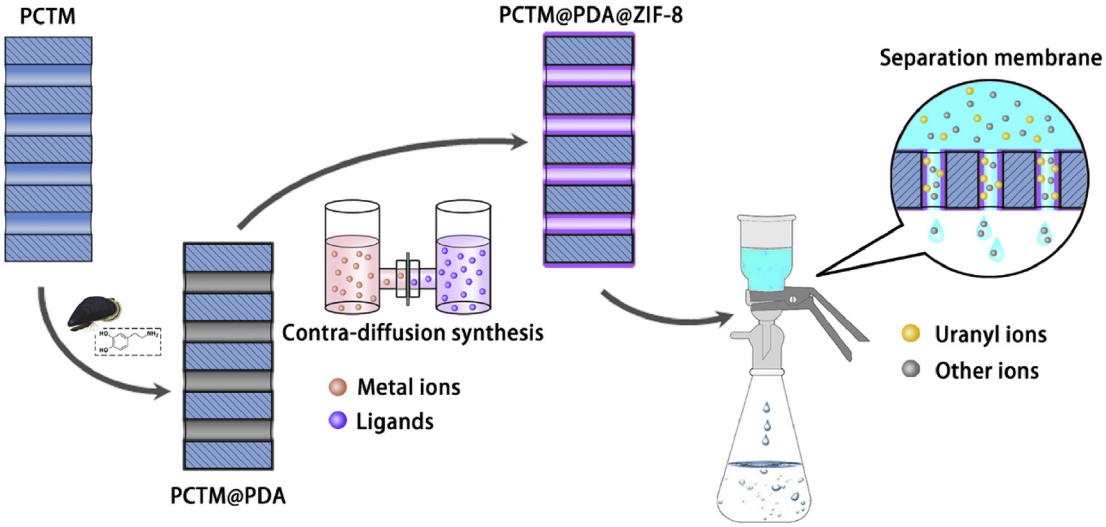

Scheme 1. Illustration of PDA-mediated preparation of polycarbonate track-etched membrane (PCTM) supported 1D ZIF-8 hollow superstructure arrays for uranium separation.

mechanism involved synergistic effect, rather than traditional coordination (Wu et al., 2014) and hydrogen bonding (Zhang et al., 2014) mechanism found in short-term adsorption experiments (Min et al., 2017), was revealed which was responsible for the entrapment of uranyl ions in the ZIF-8 superstructure arrays.

2. Materials and methods

2.1. Materials

Sodium hydroxide (98%), zinc nitrate hexahydrate (99.5%), sodium carbonate (99%), sodium perchlorate (98%), dichloromethane (99.5%, AR) were bought from Beijing Chemical Works. Dopamine hydrochloride (DA, 98%), methanol (99.9%, ACS/HPLC certified), ethanol (99.9%, ACS/HPLC certified), 2-methylimidazole (99%), tartaric acid (99%), arsenazo III (95%) were supplied by J&K Scientific Co., Ltd. Tris(hydroxymethyl)aminomethane (Tris) (>99%) and sodium perchlorate (>98%) were purchased from Sigma-Aldrich. Deionized water was used for the preparation of all aqueous solutions. All reagents were used as received without further purification. Polycarbonate (PC) membranes were purchased from Bayer Company. A standard stock solution of U(VI) (100 mg/L) and uranyl nitrate hexahydrate $UO_2(NO_3)_2 \cdot 6H_2O$ were provided by the China Institute of Atomic Energy.

2.2. Preparation of PCTMs

The polycarbonate track-etched membranes were prepared according to our previously reported method (Yuan et al., 2016). PC membranes with a thickness of 10 μm were irradiated on a heavy ion accelerator with Kr^{84} ions, and stored at room temperature for more than one month. After that, the irradiated PC membrane were exposured to ultraviolet (UV) light for 1 h on each side, and then fixed on a mould and immersed in 6.25 mol/L NaOH solution, etching at 50 °C under stirring condition for 10 min. The obtained PCTMs were rinsed three times with deionized water under ultrasonication and then dried at room temperature.

2.3. PDA modification of the pore channels of PCTM

A piece of the as-prepared PCTM was fixed on a mould and rinsed with deionized water, followed by immersion into 10 mM Tris-HCl (pH = 8.5) buffer. Vacuum treatment was implemented to expel the air present in the pores, until no bubbles appeared on membrane. Dopamine hydrochloride solution was added dropwise into the buffer with sufficient stirring (200 rpm) on both sides of the PCTM, until the concentration of dopamine in buffer reached 1 g/L. The modification process lasted for 8 h at room temperature, and then the obtained PDA modified PCTM was rinsed in deionized water with ultrasonication, dried in a vacuum oven at 50 °C.

2.4. Synthesis of ZIF-8 crystal

Zinc nitrate hexahydrate (297 mg, 1 mmol) and 2-methylimidazole (328 mg, 4 mmol) were dissolved in 20 mL methanol, respectively. The two solutions were mixed together at room temperature under magnetic stirring for 12 h to obtain white colloidal suspension. After repeated centrifugation of reaction mixture and washed by methanol for 3 times, the ZIF-8 were dried under vacuum at 50 °C.

2.5. Contra-diffusion synthesis of ZIF-8 within PCTM pore channels

ZIF-8 was in-situ grown within the pore channels of the PDA modified PCTMs *via* a contra-diffusion method (He et al., 2013; Yao et al., 2011). 1 mmol $Zn(NO_3)_2 \cdot 6H_2O$ and 4 mmol 2-methylimidazole were dissolved in 20 mL methanol, respectively. A piece of PDA modified PCTM was then immersed in the $Zn(NO_3)_2$/methanol solution for 30 min following by slight dipping in methanol, pre-coordinating the PDA coating with Zn^{2+}. Next, the PCTM was placed between the two chambers of a contra-diffusion cell, while $Zn(NO_3)_2$ and 2-methylimidazole solution were synchronously added into different chambers. After 1 h contra-diffusion synthesis, the functionalized PCTM was dipped in methanol several times to wash off the loose crystals on the surface and dried under vacuum at 50 °C. The self-supporting 1D ZIF-8 hollow superstructures array was obtained by dissolving the matrix membrane in dichloromethane, followed by repeated centrifuging and washing in methanol and finally dried under vacuum at 50 °C.

2.6. Uranium separation

Adsorption of uranium by native ZIF-8 and PCTM supported ZIF-8 superstructures were firstly implemented by batch operation in Erlenmeyer flask. Typically, a certain amount of adsorbent were mixed with uranium solution, followed by magnetic stirring at room temperature. The initial pH value of the uranium solutions was adjusted by adding HNO_3 and/or NaOH aqueous solutions (negligible volume). The ionic strength of the solutions was maintained using 0.01 mol/L $NaClO_4$. When adsorption equilibrium was reached, the adsorbent were filtrated through a 0.22 μm membrane filter (for native ZIF-8) or removed directly (for membrane), and the concentration of residual U (VI) in aqueous phase was measured by ICP-AES.

Uranium separation by PCTM supported ZIF-8 superstructures was also comparatively performed by filtration in a flow-through mode. A piece of membrane was placed on a porous glass support fixed by a clamp and a certain amount of uranium solution was introduced. The concentration of residual uranium after filtration was measured by ICP-AES.

Adsorption capacity q (mg/g) and removal rate R (%) are defined as follows:

$$q = \frac{C_0 - C_e}{m} \times V \quad (1)$$

$$R(\%) = \frac{C_0 - C_e}{C_e} \times 100 \quad (2)$$

where C_0 (mg/L) and C_e (mg/L) are the initial and residual U(VI) concentration in the aqueous solutions, respectively. V is the volume of the initial solution and m is the weight of the adsorbent.

2.7. Characterizations

Scanning electron microscope (SEM) was conducted by using ZEISS MERLIN and FEI QUANTA 200 scanning electron microscope. The sample was disposed with metal or carbon spraying before observation. It was observed at an accelerating voltage of 30 kV in vacuum condition after metal spraying. Transmission electron microscopy (TEM) images were recorded by using a model H-7700 microscope with an accelerating voltage of 120 kV. Fourier transform infrared (FT-IR) spectra were recorded on Nicolet iN10 Infrared Microscope. Powder X-ray diffraction (XRD) patterns were obtained on a diffractometer with Cu Kα radiation, with a scan step of 0.2° and the scan range between 3° and 50°. Nitrogen adsorption-desorption isotherms were measured by a NOVA 3200e Surface Area & Pore Size Analyzer. Samples were dried at 80 °C (for PCTMs) under vacuum for at least 3 h before the nitrogen adsorption experiments. Specific surface areas were calculated based

upon the Brunauer-Emmett-Teller (BET) method. The surface chemistry and composition analysis of the samples were examined with a model 250XI X-ray photoelectron spectroscopy (XPS) spectrometer equipped with a mono Al Kα X-ray source (1361 eV). Elemental analysis of C, H, N and O was performed on an Elementar Vario EL III instrument. Thermogravimetric analysis (TGA) was conducted on a TA Instruments SDT Q600 instrument at a heating rate of 10 °C/min from 50 to 1000 °C. Samples weighing ~5 mg were heated in a N_2 flow (100 mL/min). The concentration of uranium and other metal ions was measured by inductively coupled plasma-atomic emission spectrometry (ICP-AES, SPECTRO ARCOS SOP).

3. Results and discussion

This work aims to develop a new approach to prepare membrane supported MOF hollow superstructures by utilizing a PDA mediated contra-diffusion synthetic strategy for uranium separation. The preparation route of PCTM supported ZIF-8 array is illustrated in Scheme 1. First, a piece of PCTM with well-defined cylindrical pores is treated by PDA deposition *via* the oxidant-controlled polymerization of dopamine, generating active modified layer on the inner surfaces of the pore channels of PCTM. Then, regulated by the PDA active layer as well as the polycarbonate matrix, in-situ nucleation and growth of ZIF-8 occurs along the pore walls with uniform thickness, forming 1D ZIF-8 hollow superstructure array arranged in the pores of PCTM. With ZIF-8 array immobilized in the pore channels of PCTM, the obtained composite is expected to be capable for facile removal of uranium from aqueous solution in a flow-through mode.

Deposition of PDA into the inner surfaces of pore channels of PCTM is to create anchoring sites of the ZIF-8 crystals while regulating their growth behavior. Meanwhile, the robust PDA interface between the polycarbonate matrix and MOFs helps to improve the structural stability of the obtained composite membranes. Fig. S1 shows the surface and section view SEM images of PCTM before and after PDA treatment. No obvious changes or decrease of pore size was observed for the well-preserved pore channels. Only some small-sized PDA aggregates were found deposited on the surface of PCTM without blocking the pore openings. Dissolving the PCTM in dichloromethane, conformal PDA nanotubes replicating the dimension of pore channels with a thickness of *ca.* 14 nm were observed under TEM (Fig. S2), indicating the generation of uniform PDA layers in the pore channels.

Then, the PDA modified layer on the pore walls of PCTM served as an active platform for contra-diffusion synthesis of ZIF-8 to fabricate membrane supported MOF superstructure array. Previous studies have proved that the existence of abundant functional groups such as catechol and amine in PDA makes it capable to coordinate the metal ions that consists of MOFs (Zhao et al., 2014; Zhou et al., 2015). Here, by pre-coordination with Zn^{2+}, a uniform nucleation layer of ZIF-8 was generated on PDA in the pore channels. Associated with the polycarbonate catalyzed transesterification mechanism during contra-diffusion synthesis, 2-methylimiazole anions, the key species to promote the nucleation and growth of ZIF-8, were generated continuously near the pore walls and coordinated to the Zn^{2+} on PDA layer, forming ordered array of ZIF-8 hollow superstructures spanning across the PCTM. The surface SEM view of ZIF-8 grown PCTM (Fig. 1a) shows a decrease in pore size and the section view (Fig. 1b) displays the well-developed ZIF-8 arrays with homogeneous distribution in the pore channels. The ZIF-8 hollow nanotubes generated within the membrane matrix can be clearly observed in the high-magnification SEM image (Fig. 1c). After dissolving the PCTM, self-supported 1D ZIF-8 hollow nanotube arrays with identical length (*ca.* 20 μm) equivalent to the thickness of the PCTM and an aspect ratio up to 40 were obtained (Fig. 1d). Fig. 1e and f show the open cavities and hollow structures of the ZIF-8 array, confirming that the pore channels of PCTM were not blocked during contra-diffusion synthesis of ZIF-8. The energy dispersive X-ray (EDX) spectroscopic mapping of corresponding elements on section of composite membrane also confirms the successful in-situ growth of ZIF-8 in the pore channels.

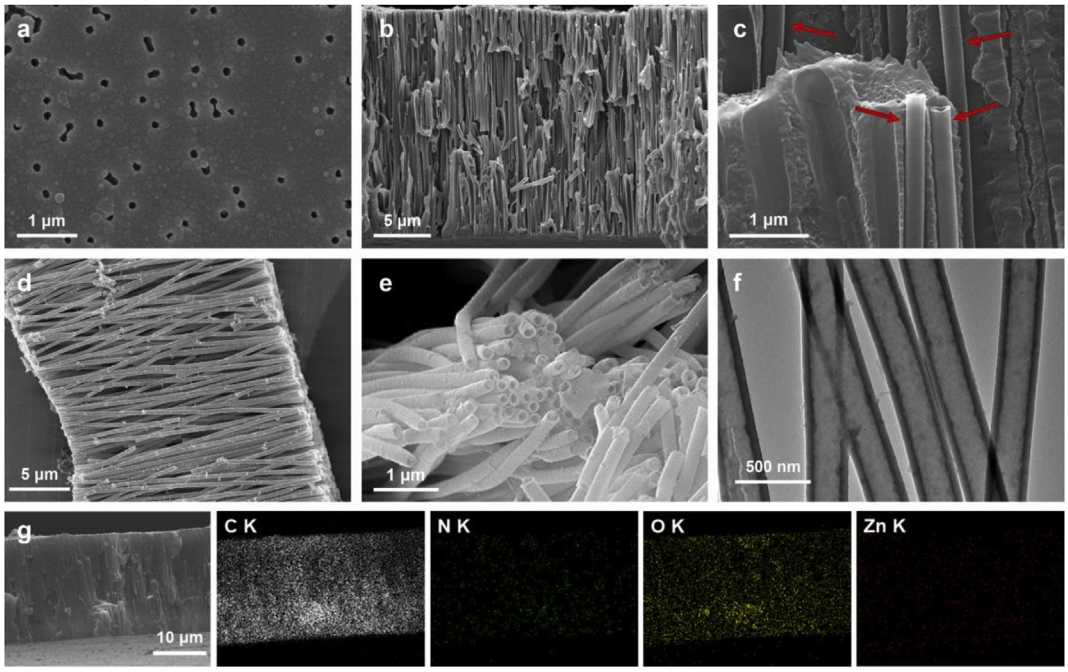

Fig. 1. Surface (a) and section view (b, c) SEM images of ZIF-8 composited PCTM; SEM (d, e) and TEM (f) images of the self-supporting 1D ZIF-8 hollow superstructures array after matrix membrane dissolution; SEM image and corresponding EDX elemental mapping of ZIF-8 composited PCTM (g).

Further evidence is provided in Fig. 2 to prove the successful fabrication of the PCTM supported ZIF-8 superstructures. Fig. 2a shows the XRD spectra of ZIF-8 crystals and the composite membranes in different stages of the fabrication process. No obvious difference was observed on spectra of PCTM and PCTM@PDA samples while the obvious diffraction peaks of ZIF-8 appeared after contra-diffusion synthesis on membrane. In the FT-IR spectra (Fig. 2b), the PCTM@PDA sample shows characteristic peak at 1601 cm^{-1} corresponding to the bending vibration of aromatic rings while the broad peak over 3000 cm^{-1} is attributed to the O–H and N–H stretching vibrations, which belongs to PDA structure. After the contra-diffusion synthesis, the resulting composite membrane, labelled as PCTM@PDA@ZIF-8, exhibits characteristic bands in the spectral region of 1411 cm^{-1} and 1307 cm^{-1} assigned to the plane stretching and bending of imidazole ring, respectively. The absorbance at 3136 cm^{-1} and 2931 cm^{-1} was attributed to the aromatic and aliphatic C–H stretching vibrations of the 2-methylimidazole ligands (Hachuła et al., 2010). XPS was used to examine the surface chemistry of composite membranes and native ZIF-8. According to the wide scan XPS spectrum in Fig. 2c, the pristine PCTM shows C 1s and O 1s signals. After PDA chemistry treatment, evident N 1s peak shows up, which is associated with the amine species in PDA structure. With the in-situ synthesis of ZIF-8 in membrane a strong Zn 2p signal can be observed in the spectrum of the PCTM@PDA@ZIF-8. The corresponding atom% is listed in Table S1, where the surface chemical composition of PCTM@PDA@ZIF-8 is close to the native ZIF-8 crystals, suggesting the coverage of ZIF-8 on the surface of composite membranes. All of the evidence indicates the successful PDA deposition and subsequent in-situ synthesis of ZIF-8 in the pore channels of membranes.

N_2 sorption-desorption experiment (Fig. 2d and Table 1.) shows a slight increase of BET specific surface area, from 13 m^2/g to 20 m^2/g, of PCTM after PDA deposition and a significant (128 m^2/g) increase after ZIF-8 growth. Compared to the BET specific surface area of native ZIF-8 (1379 m^2/g), it can be roughly estimated that about 8.0 wt% of ZIF-8 was grown in the pore channels of the membrane. Considering the fact that the decrease of crystal size and the aggregation of nanocrystals have negative effect on crystalline, resulting in the decrease of porosity, this loading amount may be lower than the real value. TGA was used to study the thermal stability of the PCTM supported ZIF-8 composites and examine their composition (Fig. 2e). The pristine PCTM exhibits a typical thermal degradation behavior of polycarbonate with a decomposition temperature (T_d) of ~478 °C. Increased weight loss is observed for the PDA modified intermediate, which shows a ~3 °C shift of T_d to relatively lower temperature because of the earlier decomposition of PDA than PCTM. With the in-situ synthesis of ZIF-8, the composite membrane shows less weight loss compared to the PDA modified intermediate. The in-situ synthesis of ZIF-8 catalyzed by transesterification mechanism results in a limited degradation of PCTM matrix, which decreases the mechanical strength of matrix and shifts T_d to a relatively lower temperature (~429 °C). Because the weight loss of ZIF-8 begins at ~600 °C and never achieves a balance (Fig. S3), 580 °C is chosen to calculate the loading amount. The loading of ZIF-8 is estimated to be 9.2 wt% that is slightly higher than the value calculated from the data of porosity.

Elemental analysis C, H, N, and O was performed to quantify the loading amount of ZIF-8 to the composite membrane. The data summarized in Table 2 show that the PCTM@PDA sample contains 0.15 wt% nitrogen and 20.21 wt% oxygen. With the introduction of

Table 1
BET specific surface areas and pore volume of composite membranes and native ZIF-8 crystals.

Samples	Specific surface area (m^2/g)	Pore volume (cm^3/g)
PCTM	13	0.03
PCTM@PDA	20	0.04
PCTM@PDA@ZIF-8	128	0.09
ZIF-8	1379	0.69

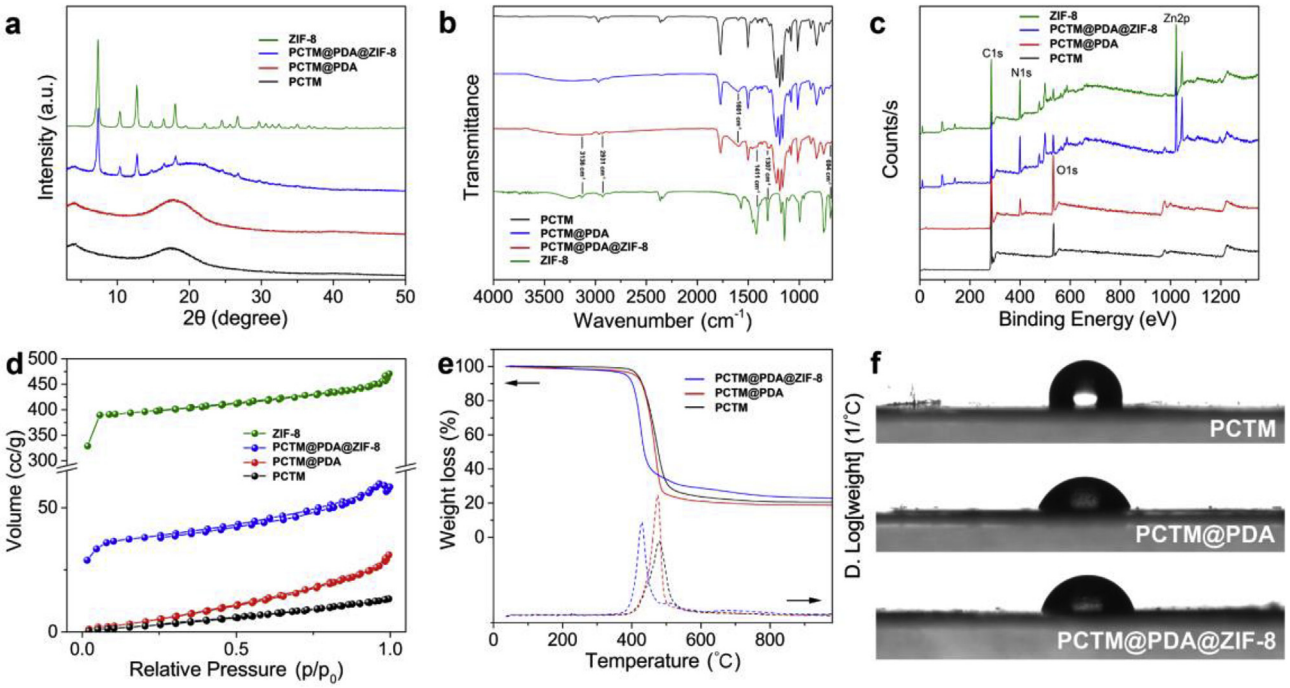

Fig. 2. Structural characterizations of ZIF-8 and membranes. XRD spectra (a), FT-IR spectra (b), wide scan XPS spectra (c), N_2 sorption-desorption isotherms (d), TGA curves and DTG plots (e) of pristine PCTM (black), PCTM@PDA (red), PCTM@PDA@ZIF-8 composites (blue), and native ZIF-8 crystals (olive), respectively; water contact angle measurements on pristine PCTM, PCTM@PDA and PCTM@PDA@ZIF-8 (f). (For interpretation of the references to colour in this figure legend, the reader is referred to the Web version of this article.)

Table 2
Elemental analysis of the composite membranes and native ZIF-8 crystals.

Samples	Elemental analysis (*wt.* %)			
	C	H	N	O
PCTM	74.73	5.31	0.02	19.94
PCTM@PDA	74.13	5.51	0.15	20.21
PCTM@PDA@ZIF-8	71.48	5.42	2.49	18.10
ZIF-8	42.42	4.44	22.16	0.22

ZIF-8, composite membranes shows increase of nitrogen to 2.49 wt % and decrease of oxygen to 18.10 wt %, respectively. Based upon the element composition of native ZIF-8, it can be estimated that approximately 10.63 wt % (calculated by N) or 10.44 wt % (calculated by O) of ZIF-8 was grown in the pore channels of the membranes.

The hydrophilicity of the composite membranes is examined by water contact angle (WCA) measurements (Fig. 2f). Pristine PCTM shows a hydrophobic surface with a WCA of 97.9°. After PDA deposition, the abundant catechol hydroxyl and amine groups in PDA improved the hydrophilicity of the modified membrane with a WCA of 67.1°. Though the WCA slightly increased to 74.1° after ZIF-8 deposition, it was still more hydrophilic than pristine PCTM. The enhancement of hydrophilicity would promote the mass transport and anti-clogging ability, resulting in better performance of the composite membranes for separation applications in aqueous environment.

Before evaluating the performance of the PCTM supported ZIF-8 hollow superstructure array for uranium entrapment, the adsorption behaviors of native ZIF-8 powder crystals toward uranyl ions were studied for probing the underline adsorption mechanism. First, the effect of pH, ranging from 2 to 6, on the uranium adsorption of ZIF-8 was investigated. As shown in Fig. S4, the peak value of capacity appears at pH = 4. Therefore, the following experiments of uranium adsorption behavior were implemented under this condition unless otherwise noted. The adsorption capacity of uranium by ZIF-8 as a function of equilibrium concentration (C_e) in solution was obtained to study the adsorption isotherm (Fig. 3a), where the initial concentrations of uranium were varied from 10 mg/L to 200 mg/L. The adsorption capacity increases rapidly at low C_e without approaching to an equilibrium within ranges of C_e. The Langmuir and Freundlich adsorption isotherm models were employed to fit the experimental data, and the calculated parameters are listed in Table S2. Apparently, the Freundlich model gives a better fitting result with a higher correlation coefficient R^2 of 0.984 and a 1/n of 0.37, suggesting multiple binding sites with the highest strength sites binding the sorbate first and a relatively complicated adsorption mechanism (Kilincarslan and Akyil, 2005).

In order to investigate the adsorption rate of uranium on the ZIF-8 crystals, the adsorption experiments at different contact times were carried out at the initial concentration of uranium of 20 ppm. The curve in Fig. 3b shows a fast adsorption kinetics of ZIF-8, reaching greater than 90% of equilibrium capacity within 30 min. The adsorption procedure can be well fitted with the pseudo-second-order kinetic model with a calculated equilibrium capacity of 266.9 mg/g, as listed in Table S3, indicating the adsorption kinetics might be dependent on a surface chemisorption reaction (Yi-Nan et al., 2013). The selectivity of the ZIF-8 to uranium against interfering metal ions was also evaluated. As shown in Fig. S5 and Table S4, ZIF-8 presents selective binding ability to uranium in the presence of 8 different interfering ions with a satisfactory capacity of 183.0 mg/g, which is a promising adsorbent for the efficient recovery of uranium from aqueous environment.

However, it should be pointed out that, with the prolonging of contact time over 2 h, the capacity of uranium presents a continuous fluctuation and increase in kinetics experiment. To explain the phenomena, the concentration of zinc ions in solution was monitored during the adsorption procedure. As shown in Fig. 3c, companied by the fluctuation of uranium concentration, a dramatic increase in zinc ions concentration was found. This implies that the adsorption of uranyl ions to ZIF-8 might be dominated by an ion-exchange mechanism (Weiting et al., 2013) in a long-term procedure, rather than the traditional coordination or hydrogen binding mechanism (Min et al., 2017).

In order to verify the hypothesis and explain the interaction between uranium and ZIF-8, the native ZIF-8 crystal and the counterparts exposed to uranium solution for different time were examined by detailed analysis of the XPS spectra. To eliminate interference of weak interactions, the samples were washed with deionized water and dried under vacuum before the test. According to the wide scan XPS spectra in Fig. 4a, native ZIF-8 shows obvious C 1s, N 1s, O1s and Zn 2p signals. After uranium adsorption, evident U 4f peaks show up at around 392 eV and 380 eV. The intensity of peaks is increased with the prolonging of time while the peaks intensity of other element remains unchanged, indicating the accumulation of uranium on ZIF-8. High-resolution N 1s and O 1s with deconvolution analysis are presented in Fig. 4b–d. The N 1s region was fitted with two main components assigned to oyxnitride (N–Zn–O, 398.3 eV) and aromatic amine (=N-, 398.9 eV) species, and two minor components assigned to primary amine (-NH_2, 401.0 eV) and secondary amine (-NH-, 400.0 eV). The minor components can be attributed to negligible protonated nitrogen on imidazole rings. In the case of native ZIF-8, the dominant aromatic

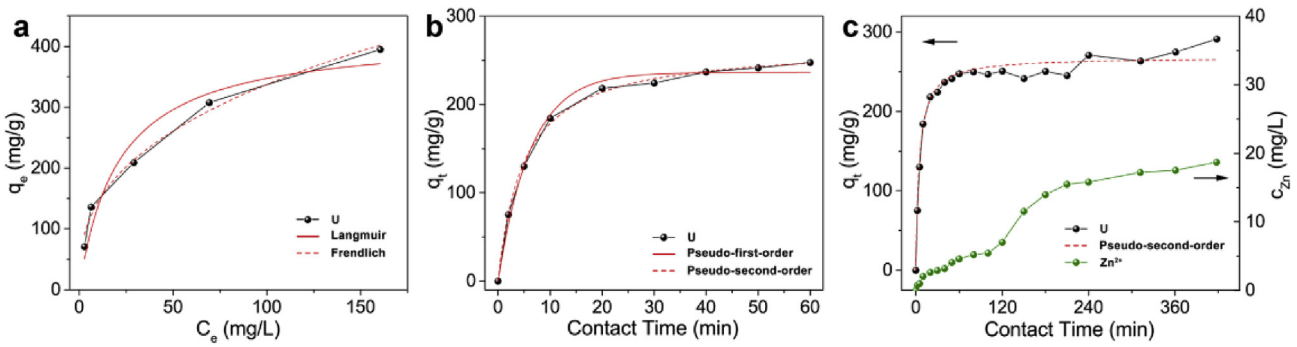

Fig. 3. Investigation on uranium adsorption behaviors of native ZIF-8. (a) Uranium adsorption isotherm fitted by the Langmuir and Freundlich models, contact time = 2 h, [m/V] = 0.1 g/L; (b) uranium adsorption kinetics curve fitted by the pseudo-first-order and pseudo-second-order model, initial concentration = 20 ppm, [m/V] = 0.025 g/L; (c) prolonging contact time of kinetics curve and the concentration curve of Zn^{2+} in solution.

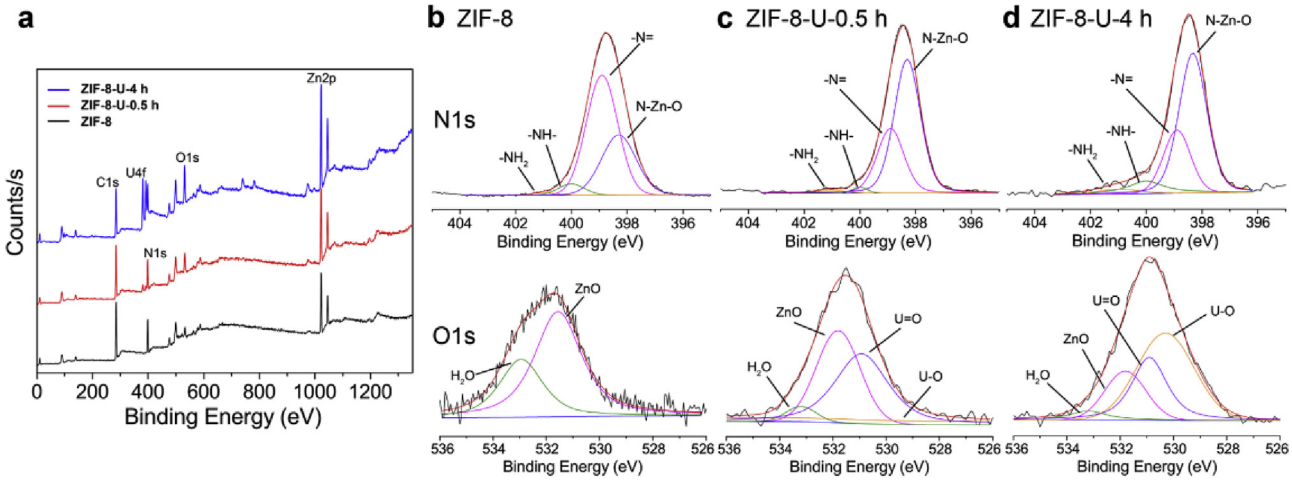

Fig. 4. Wide scan XPS spectra of native ZIF-8 and ZIF-8 exposed to uranium-containing solution for short-term (0.5 h) and long-term (4 h) (a); high-resolution XPS spectra of N 1s and O 1s regions for native ZIF-8 (b) and ZIF-8 exposed to uranium-containing solution for 0.5 h (c) and 4 h (d).

amine belongs to the nitrogen in imidazole ring, while the N—Zn—O species are associated with the H_2O-involved coordination of nitrogen and zinc ions (Li et al., 2014). After uranium adsorption for 0.5 h, the N—Zn—O became the dominant species, which was associated with the process that H_2O molecules were replaced by uranyl ions coordinating with nitrogen on surface of ZIF-8. The deconvolution results show no obvious difference when the contact time was prolonged to 4 h, suggesting the coordination mechanism throughout the adsorption process. The O 1s region was fit with four peaks corresponding to H_2O (532.9 eV), Zn—O (531.5 eV), U═O (530.3 eV), and U—O (530.9 eV) species. Due to the native ZIF-8 containing no oxygen, the signal is corresponding to the H_2O capture by crystal lattice and the oxidation of zinc ions on the surface of ZIF-8, respectively (Tian et al., 2015). After exposure to uranium for 0.5 h, evident uranyl ions peak (U═O) shows up because of the coordination of uranyl ions on ZIF-8. But when the time was prolonged to 4 h, the U═O species shifted to relatively lower binding energy region and, in some ways, translated into U—O species (Schindler et al., 2009), which can be interpreted as some uranyl ions enter into the crystal lattice of ZIF-8 and exchange with the zinc ions. Such theory explains the release of zinc ions on long-term adsorption process, implying the combined actions of coordination and ion-exchange mechanism of uranium adsorption on ZIF-8. In addition, the C 1s region was fit with three peaks

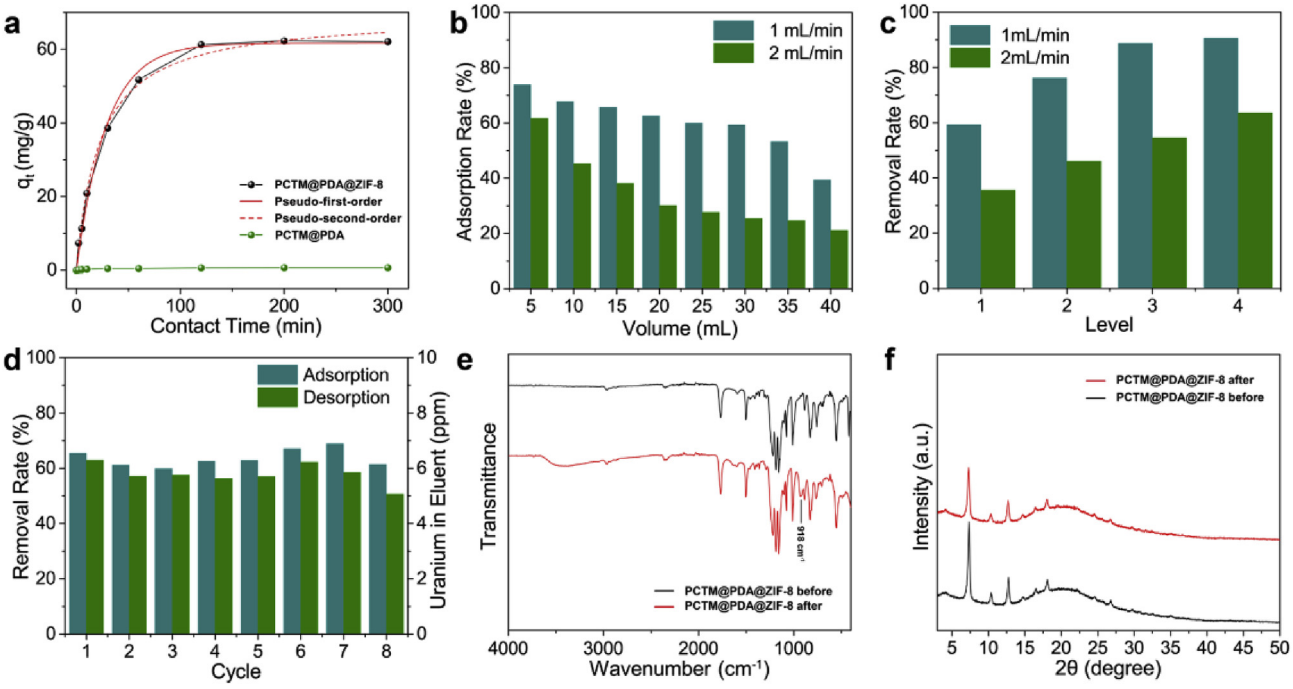

Fig. 5. Investigation on uranium separation performance of PCTM supported ZIF-8 hollow superstructure array. (a) Uranium adsorption kinetics curve of in batch experiment fitted by the pseudo-first-order and pseudo-second-order model; uranium sample: 20 ppm, [m/V] = 0.075 g/L. (b) Effect of flow velocity on the breakthrough curve for uranium filtration adsorption, [U(VI)] = 10 ppm. (c) Effect of flow velocity on the multi-stage filtration, [U(VI)] = 10 ppm, 10 mL. (d) Uranium removal rate and elution amount in eight adsorption-desorption filtration cycles; [U(VI)] = 10 ppm, 10 mL; eluent: 0.1 mol/L Na_2CO_3 solution, 10 mL. FT-IR (e) and XRD (f) spectra of the PCTM supported ZIF-8 hollow superstructure array before and after uranium adsorption on filtration experiment.

assigned to C–O, C=O and C–C/C=C, as shown in Fig. S6. The spectra of C 1s present few changes after exposed to uranium, suggesting no interaction between C and uranyl ions.

The performance of PCTM supported ZIF-8 hollow superstructure array for uranium separation was mainly evaluated in a flow-through mode. Prior to that, traditional batch adsorption experiment, as a comparative study, was carried out. The effective area of membrane is presented in Fig. S7, which is a circle area with a diameter of 1.2 cm. Fig. 5a shows the adsorption kinetics curves in batch experiments of the ZIF-8 composite membrane and its parent intermediate PCTM@PDA. It is clearly that without ZIF-8 functional layer, the membrane shows almost no affinity to uranium. The kinetics curve of ZIF-8 composite membrane was fitted well by both pseudo-first-order and pseudo-second-order model, showing a correlation coefficient R^2 of 0.994 and 0.995 (Table S5), respectively. Compared with the kinetics of native ZIF-8, it can be explained by the diffusion of uranyl ions was limited by the structure of membrane, reducing the concentration of uranium in pore channels, which, in some degree, turns surface chemisorption controlled mechanism into diffusion controlled mechanism (Wu et al., 2017).

The breakthrough curves of ZIF-8 composite membrane in flow-through mode are presented in Fig. 5b. At flow velocity of 1 mL/min, the composite membrane can treat 30 mL uranium-containing water without an obvious decrease of removal rate, showing a handling capacity of 265 L/m^2 for single level. It is worth mentioning that the removal rate is greatly dependent on flow velocity. When the flow velocity increase to 2 mL/min, a relatively fast decrease in removal rate is observed, which can be attributed to the decrease of contact time and the collapse of ZIF-8 functional layer. The effect of flow velocity on uranium separation performance of the composite membrane is also shown in multi-stage filtration experiment (Fig. 5c). The removal rate rises to over 90% after four levels filtration at the flow velocity of 1 mL/min. However, only 60% removal rate is achieved after four levels at the flow velocity of 2 mL/min, which is nearly equal to the performance of one level filtration at 1 mL/min. For the recovery of uranium and the regeneration of the composite membrane, 0.1 mol/L sodium carbonate solution was selected as eluent. As Fig. 5d shown, the uranium can be rapidly released out after an easy flow-through elution, and the elution amount keeps slightly lower than adsorbed amount. With the eluent of Na_2CO_3 solution, the composite membrane can be reuse for seven times without an obvious performance degradation. The removal rate shows a tendency of increase first and then decrease, which is speculated to be attributed to the ion-exchange mechanism. In the first three cycles, the residual uranium after elution occupy the adsorption site on ZIF-8 surface, resulting the decrease of removal rate. With the increase of contact time, the residual uranium enter into crystal lattice and release the adsorption site for more uranium. What's more, because of the ZIF-8 functional layer assembled by nanocrystal, the intercrystalline adsorption sites require more time to be reach by uranyl ions. These factors result in the increase of removal rate from forth to seventh cycles. After seven cycle of adsorption-desorption, both removal and elution rates show a sharp decrease, suggesting the performance degradation of the composite membrane. FT-IR and XRD were used to characterize the structure of composite membrane after uranium adsorption. The FT-IR result (Fig. 5e) shows an intense peak appeared at 918 cm^{-1} with the other peaks keep unchanged, confirming the presence of uranium species and the stability of composite membrane after adsorption. The same XRD patterns (Fig. 5f) of composite membrane before and after uranium adsorption also proves the structural stability. Meanwhile, the SEM and TEM images (Fig. S8) of ZIF-8 composite membrane and self-supporting 1D ZIF-8 hollow superstructures after uranium adsorption show no obvious changes on morphologies compared to those in Fig. 1, further confirming the structural stability of the ZIF-8 composite membranes.

4. Conclusions

In this work, by taking advantage of the PDA chemistry mediated contra-diffusion synthetic strategy, robust membrane supported 1D ZIF-8 hollow superstructures were developed for facile separation of uranium in a filtration mode. The PDA functional layer deposited on the inner surfaces of the pore channels regulated the heterogeneous nucleation and interfacial growth of the ZIF-8 crystals, enabling the architecture of 1D ZIF-8 hollow superstructures integrated with the PCTM matrix. These membrane supported 1D MOF hollow superstructures represents a novel class of organic-inorganic composite membrane, which then served as micro-scaled chromatographic column arrays for effective entrapment of uranium from aqueous solutions. The outstanding performance for uranium separation was demonstrated in both batch mode and fast flow-thought mode. New insights into the interaction between ZIF-8 and uranyl ions were obtained, suggesting that an ion-exchange mechanism, combined with coordination interaction, was responsible for the adsorption of uranium, especially in a long-term exposure. Besides, the ZIF-8 composite membranes could be regenerated by sodium carbonate solution in flow-through mode and showed great reusability on uranium filtration adsorption. This makes the composite membranes promising for the separation of uranium from aqueous environment. Considering the adaptable coordination of PDA to various metal ions, we believe that the methodology developed in this study is versatile for preparing more MOF superstructures with deployable form for broadened applications.

Conflicts of interest

The authors declare there is no conflicts of interest regarding the publication of this paper.

Acknowledgments

The study was financially supported by the Changjiang Scholars and Innovative Research Team in University (IRT13026), the National Science Fund for Distinguished Young Scholars (51425403), National Natural Science Foundation of China under Project 51673109 and 51473087.

Appendix A. Supplementary data

Supplementary data to this article can be found online at https://doi.org/10.1016/j.envpol.2019.06.114.

References

Abney, C.W., Mayes, R.T., Saito, T., Dai, S., 2017. Materials for the recovery of uranium from seawater. Chem. Rev. 117, 13935–14013.
Al-Maythalony, B.A., Alloush, A.M., Faizan, M., Dafallah, H., Elgzoly, M.A.A., Seliman, A.A.A., Al-Ahmed, A., Yamani, Z.H., Habib, M.A.M., Cordova, K.E., Yaghi, O.M., 2017. Tuning the interplay between selectivity and permeability of ZIF-7 mixed matrix membranes. ACS Appl. Mater. Interfaces 39, 33401–33407.
Apel, P., 2001. Track etching technique in membrane technology. Radiat. Meas. 34, 559–566.
Bone, S.E., Dynes, J.J., Cliff, J., Bargar, J.R., 2017. Uranium(IV) adsorption by natural organic matter in anoxic sediments. Proc. Natl. Acad. Sci. U. S. A. 114, 711–716.
Chen, L., Bai, Z., Zhu, L., Zhang, L., Cai, Y., Li, Y., Liu, W., Wang, Y., Chen, L., Diwu, J., Wang, J., Chai, Z., Wang, S., 2017. Ultrafast and efficient extraction of uranium from seawater using an amidoxime appended metal-organic framework. ACS Appl. Mater. Interfaces 9, 32446–32451.
Chizallet, C., Lazare, S., Bazerbachi, D., Bonnier, F., Lecocq, V., Soyer, E., Quoineaud, A.A., Bats, N., 2010. Catalysis of transesterification by a non-functionalized metal-organic framework: acido-basicity at the external surface

of ZIF-8 probed by FTIR and ab initio calculations. J. Am. Chem. Soc. 132, 12365–12377.
Chu, S., Majumdar, A., 2012. Opportunities and challenges for a sustainable energy future. Nature 488, 294–303.
Cui, X., Chen, K., Xing, H., Yang, Q., Krishna, R., Bao, Z., Wu, H., Zhou, W., Dong, X., Han, Y., 2016. Pore chemistry and size control in hybrid porous materials for acetylene capture from ethylene. Science 353, 141–144.
Dargahi, R., Ebrahimzadeh, H., Asgharinezhad, A.A., Hashemzadeh, A., Amini, M.M., 2017. Dispersive magnetic solid-phase extraction of phthalate esters from water samples and human plasma based on a nanosorbent composed of MIL-101(Cr) metal-organic framework and magnetite nanoparticles before their determination by GC-MS. J. Sep. Sci. 41, 948–957.
Deria, P., Gomez-Gualdron, D.A., Hod, I., Snurr, R.Q., Hupp, J.T., Farha, O.K., 2016. Framework-topology-dependent catalytic activity of zirconium-based (Porphinato)zinc(II) MOFs. J. Am. Chem. Soc. 138, 14449–14457.
Ehrling, S., Kutzscher, C., Freund, P., Müller, P., Senkovska, I., Kaskel, S., 2018. MOF@SiO 2 core-shell composites as stationary phase in high performance liquid chromatography. Microporous Mesoporous Mater. 263, 268–274.
Falcaro, P., Ricco, R., Doherty, C.M., Liang, K., Hill, A.J., Styles, M.J., 2014. MOF positioning technology and device fabrication. Chem. Soc. Rev. 43, 5513–5560.
Feng, Y., Jiang, H., Li, S., Wang, J., Jing, X., Wang, Y., Chen, M., 2013. Metal–organic frameworks HKUST-1 for liquid-phase adsorption of uranium. Colloid. Surf. A Physicochem. Eng. Asp. 431, 87–92.
Fleischer, R.L., Price, P.B., 1964. Techniques for geological dating of minerals by chemical etching of fission fragment tracks. Geochim. Cosmochim. Acta 28, 1705–1714.
Furukawa, S., Reboul, J., Diring, S., Sumida, K., Kitagawa, S., 2014. Structuring of metal-organic frameworks at the mesoscopic/macroscopic scale. Chem. Soc. Rev. 43, 5700–5734.
Gill, G.A., Kuo, L.J., Janke, C.J., Park, J., Jeters, R., Bonheyo, G., Pan, H.B., Wai, C.M., Khangaonkar, T., Bianucci, L., 2016. The uranium from seawater program at PNNL: overview of marine testing, adsorbent characterization, adsorbent durability, adsorbent toxicity, and deployment studies. Ind. Eng. Chem. Res. 55, 4264–4277.
Hachuła, B., Nowak, M., Kusz, J., 2010. Crystal and molecular structure analysis of 2-methylimidazole. J. Chem. Crystallogr. 40, 201–206.
He, M., Yao, J., Li, L., Zhong, Z., Chen, F., Wang, H., 2013. Aqueous solution synthesis of ZIF-8 films on a porous nylon substrate by contra-diffusion method. Microporous Mesoporous Mater. 179, 10–16.
He, Y., Li, B., O'Keeffe, M., Chen, B., 2014. ChemInform Abstract: multifunctional metal—organic frameworks constructed from meta-benzenedicarboxylate units. Chem. Soc. Rev. 43, 5618–5656.
Huang, A., Liu, Q., Wang, N., Zhu, Y., Caro, J., 2014. Bicontinuous zeolitic imidazolate framework ZIF-8@GO membrane with enhanced hydrogen selectivity. J. Am. Chem. Soc. 136, 14686–14689.
Huang, H., Schwab, K., Jacangelo, J.G., 2009. Pretreatment for low pressure membranes in water treatment: a review. Environ. Sci. Technol. 43, 3011–3019.
Huang, K., Li, Q., Liu, G., Shen, J., Guan, K., Jin, W., 2015. A ZIF-71 hollow fiber membrane fabricated by contra-diffusion. ACS Appl. Mater. Interfaces 7, 16157–16160.
Jian, M., Wang, H., Liu, R., Qu, J., Wang, H., Zhang, X., 2016. Self-assembled one-dimensional MnO2@zeolitic imidazolate framework-8 nanostructures for highly efficient arsenite removal. Environ. Sci.: Nano 3, 1186–1194.
Kalmutzki, M.J., Diercks, C.S., Yaghi, O.M., 2018. Metal-organic frameworks for water harvesting from air. Adv. Mater. 1704304.
Kilincarslan, A., Akyil, S., 2005. Uranium adsorption characteristic and thermodynamic behavior of clinoptilolite zeolite. J. Radioanal. Nucl. Chem. 264, 541–548.
Knebel, A., Zhou, C., Huang, A., Zhang, J., Kustov, L., Caro, J., 2018. Smart metal-organic frameworks (MOFs): switching gas permeation through MOF membranes by external stimuli. Chem. Eng. Technol. 41, 224–234.
Koushkbaghi, S., Zakialamdari, A., Pishnamazi, M., Ramandi, H.F., Aliabadi, M., Irani, M., 2018. Aminated-Fe3O4 nanoparticles filled chitosan/PVA/PES dual layers nanofibrous membrane for the removal of Cr(VI) and Pb(II) ions from aqueous solutions in adsorption and membrane processes. Chem. Eng. J. 337, 169–182.
Lee, H., Dellatore, S.M., Miller, W.M., Messersmith, P.B., 2007. Mussel-inspired surface chemistry for multifunctional coatings. Science 318, 426–430.
Li, B., Chrzanowski, M., Zhang, Y., Ma, S., 2016. Applications of metal-organic frameworks featuring multi-functional sites. Coord. Chem. Rev. 307, 106–129.
Li, B., Leng, K., Zhang, Y., Dynes, J.J., Wang, J., Hu, Y., Ma, D., Shi, Z., Zhu, L., Zhang, D., Sun, Y., Chrzanowski, M., Ma, S., 2015. Metal-organic framework based upon the synergy of a Bronsted acid framework and Lewis acid centers as a highly efficient heterogeneous catalyst for fixed-bed reactions. J. Am. Chem. Soc. 137, 4243–4248.
Li, C., Hu, C., Zhao, Y., Song, L., Zhang, J., Huang, R., Qu, L., 2014. Decoration of graphene network with metal–organic frameworks for enhanced electrochemical capacitive behavior. Carbon 78, 231–242.
Li, J., Wang, X., Zhao, G., Chen, C., Chai, Z., Alsaedi, A., Hayat, T., Wang, X., 2018. Metal-organic framework-based materials: superior adsorbents for the capture of toxic and radioactive metal ions. Chem. Soc. Rev. 47, 2322–2356.
Li, J.R., Kuppler, R.J., Zhou, H.C., 2009. Selective gas adsorption and separation in metal-organic frameworks. Chem. Soc. Rev. 38, 1477–1504.
Liu, Q., Wang, N., Caro, J., Huang, A., 2013. Bio-inspired polydopamine: a versatile and powerful platform for covalent synthesis of molecular sieve membranes. J. Am. Chem. Soc. 135, 17679–17682.
Lu, G., Li, S., Guo, Z., Farha, O.K., Hauser, B.G., Qi, X., Wang, Y., Wang, X., Han, S., Liu, X., DuChene, J.S., Zhang, H., Zhang, Q., Chen, X., Ma, J., Loo, S.C., Wei, W.D., Yang, Y., Hupp, J.T., Huo, F., 2012. Imparting functionality to a metal-organic framework material by controlled nanoparticle encapsulation. Nat. Chem. 4, 310–316.
Maleki, A., Hayati, B., Naghizadeh, M., Sang, W.J., 2015. Adsorption of hexavalent chromium by metal organic frameworks from aqueous solution. J. Ind. Eng. Chem. 28, 211–216.
Meimei, Z., Jian, L., Meng, Z., Hui, W., Yue, L., Yi-Nan, W., Fengting, L., Guangtao, L., 2015. Polydopamine layer as nucleation center of MOF deposition on "inert" polymer surfaces to fabricate hierarchically structured porous films. Chem. Commun. 51, 2706–2709.
Min, X., Yang, W., Hui, Y.F., Gao, C.Y., Dang, S., Sun, Z.M., 2017. Fe_3O_4@ZIF-8: a magnetic nanocomposite for highly efficient UO_2^{2+} adsorption and selective UO_2^{2+}/Ln^{3+} separation. Chem. Commun. (Camb.) 53, 4199–4202.
Na, Y., Ke, W., Wang, L., Li, Z., 2016. Amino-functionalized MOFs combining ceramic membrane ultrafiltration for Pb (II) removal. Chem. Eng. J. 306, 619–628.
Norbert, S., Shyam, B., 2011. Synthesis of metal-organic frameworks (MOFs): routes to various MOF topologies, morphologies, and composites. Chem. Rev. 112, 933–969.
Peng, Y., Huang, H., Liu, D., Zhong, C., 2016. Radioactive barium ion trap based on metal-organic framework for efficient and irreversible removal of barium from nuclear waste water. ACS Appl. Mater. Interfaces 8, 8527–8535.
Płotka-Wasylka, J., Szczepańska, N., Guardia, M.D.L., Namieśnik, J., 2016. Modern trends in solid phase extraction: new sorbent media. Trends Anal. Chem. 77, 23–43.
Schindler, M., Hawthorne, F.C., Freund, M.S., Burns, P.C., 2009. XPS spectra of uranyl minerals and synthetic uranyl compounds. II: the O 1s spectrum. Geochim. Cosmochim. Acta 73, 2488–2509.
Sugasaka, K., Katoh, S., Takai, N., Takahashi, H., Umezawa, Y., 1981. Recovery of uranium from seawater. Separ. Sci. 16, 971–985.
Sun, Q., Aguila, B., Earl, L.D., Abney, C.W., Wojtas, L., Thallapally, P.K., Ma, S., 2018. Covalent organic frameworks as a decorating platform for utilization and affinity enhancement of chelating sites for radionuclide sequestration. Adv. Mater. 1705479.
Tian, F., Mosier, A.M., Park, A., Webster, E.R., Cerro, A.M., Shine, R.S., Benz, L., 2015. In situ measurement of CO2 and H2O adsorption by ZIF-8 films. J. Phys. Chem. C 119, 15248–15253.
Wang, D., Song, J., Wen, J., Yuan, Y., Liu, Z., Lin, S., Wang, H., Wang, H., Zhao, S., Zhao, X., Fang, M., Lei, M., Li, B., Wang, N., Wang, X., Wu, H., 2018. Significantly enhanced uranium extraction from seawater with mass produced fully amidoximated nanofiber adsorbent. Adv. Energy Mater. 1802607.
Wang, X., Yu, S., Wang, X., 2019. Removal of radionuclides by metal-organic framework-based materials. J. Inorg. Mater. 34, 17–26.
Weiting, Y., Zhi-Qiang, B., Wei-Qun, S., Li-Yong, Y., Tao, T., Zhi-Fang, C., Hao, W., Zhong-Ming, S., 2013. MOF-76: from a luminescent probe to highly efficient U(VI) sorption material. Chem. Commun. 49, 10415–10417.
Wu, F., Pu, N., Ye, G., Sun, T., Wang, Z., Song, Y., Wang, W., Huo, X., Lu, Y., Chen, J., 2017. Performance and mechanism of uranium adsorption from seawater to poly(dopamine)-inspired sorbents. Environ. Sci. Technol. 51, 4606–4614.
Wu, M.X., Yang, Y.W., 2017. Metal-organic framework (MOF)-Based drug/cargo delivery and cancer therapy. Adv. Mater. 29, 1606134.
Wu, Y., Pang, H., Yao, W., Wang, X., Yu, S., Yu, Z., Wang, X., 2018. Synthesis of rod-like metal-organic framework (MOF-5) nanomaterial for efficient removal of U(VI): batch experiments and spectroscopy study. Sci. Bull. 63, 831–839.
Wu, Y.N., Zhou, M., Zhang, B., Wu, B., Li, J., Qiao, J., Guan, X., Li, F., 2014. Amino acid assisted templating synthesis of hierarchical zeolitic imidazolate framework-8 for efficient arsenate removal. Nanoscale 6, 1105–1112.
Yao, J., Dong, D., Li, D., He, L., Xu, G., Wang, H., 2011. Contra-diffusion synthesis of ZIF-8 films on a polymer substrate. Chem. Commun. 47, 2559–2561.
Yi-Nan, W., Meimei, Z., Bingru, Z., Baozhen, W., Jie, L., Junlian, Q., Xiaohong, G., Fengting, L., 2013. Amino acid assisted templating synthesis of hierarchical zeolitic imidazolate framework-8 for efficient arsenate removal. Nanoscale 6, 1105–1112.
Yu, B., Ye, G., Zeng, Z., Zhang, L., Chen, J., Ma, S., 2018. Mussel-inspired polydopamine chemistry to modulate template synthesis of 1D metal–organic framework superstructures. J. Mater. Chem. A 6, 21567–21576.
Yuan, H., Lu, Y., Wang, Z., Ren, Z., Wang, Y., Zhang, S., Zhang, X., Chen, J., 2016. Single nanoporous gold nanowire as a tunable one-dimensional platform for plasmon-enhanced fluorescence. Chem. Commun. (Camb.) 52, 1808–1811.
Zhang, L., Wu, G., Jiang, J., 2014. Adsorption and diffusion of CO2 and CH4 in zeolitic imidazolate framework-8: effect of structural flexibility. J. Phys. Chem. C 118, 8788–8794.
Zhang, Z., Zaworotko, M.J., 2014. Template-directed synthesis of metal-organic materials. Chem. Soc. Rev. 43, 5444–5455.
Zhao, M., Deng, C., Zhang, X., 2014. The design and synthesis of a hydrophilic core-shell-shell structured magnetic metal-organic framework as a novel immobilized metal ion affinity platform for phosphoproteome research. Chem. Commun. (Camb.) 50, 6228–6231.
Zhe, W., Hu, S., Jian, Y., Liang, A., Li, Y., Zhuang, Q., Gu, J., 2018. Nanoscale Zr-based MOFs with tailorable size and introduced mesopore for protein delivery. Adv. Funct. Mater. 28, 1707356.
Zhou, J., Wang, P., Wang, C., Goh, Y.T., Fang, Z., Messersmith, P.B., Duan, H., 2015. Versatile core–shell nanoparticle@metal–organic framework nanohybrids: exploiting mussel-inspired polydopamine for tailored structural integration.

ACS Nano 9, 6951–6960.
Zhu, L., Sheng, D., Xu, C., Dai, X., Silver, M.A., Li, J., Li, P., Wang, Y., Wang, Y., Chen, L., Xiao, C., Chen, J., Zhou, R., Zhang, C., Farha, O.K., Chai, Z., Albrecht-Schmitt, T.E., Wang, S., 2017. Identifying the recognition site for selective trapping of (99) TcO4(-) in a hydrolytically stable and radiation resistant cationic metal-organic framework. J. Am. Chem. Soc. 139, 14873–14876.
Zhuang, J.-L., Ceglarek, D., Pethuraj, S., Terfort, A., 2011. Rapid room-temperature synthesis of metal-organic framework HKUST-1 crystals in bulk and as oriented and patterned thin films. Adv. Funct. Mater. 21, 1442–1447.